Eur Biophys J (1986) 13:175–185

European Biophysics Journal

The superstructure of chromatin and its condensation mechanism

II. Theoretical analysis of the X-ray scattering patterns and model calculations

J. Bordas[1], L. Perez-Grau[2]*, M. H. J. Koch[2], M. C. Vega[2], and C. Nave[1]

[1] MRC/SERC Biology Support Laboratory, Daresbury Laboratory, Warrington WA4 4AD, England
[2] European Molecular Biology Laboratory, c/o DESY, Notkestrasse 85, D-2000 Hamburg 52, Federal Republic of Germany

Received April 10, 1985/Accepted in revised from August 28, 1985

Abstract. Model calculations on the superstructure of uncondensed and condensed chromatin are presented. It is found that agreement between the calculated X-ray solution scattering patterns and the experimental observations can be reached with the assumptions that: a) The uncondensed chromatin fibre in solution has a helix-like structure, with a pitch of ca. 33.0 nm, a helical diameter of ca. 20.0 nm and 2.75–3.25 nucleosomes per turn. b) The most condensed state of the chromatin fibre in solution is best represented by a helix-like structure with ca. 2.56 nucleosomes per turn, a pitch of ca. 3.0 nm and a helical diameter of ca. 27.0 nm.

Key words: Chromatin superstructure, chromatin condensation

1. Introduction

In the accompanying paper and in Perez-Grau et al. (1984) we have reported the experimental results on a synchrotron radiation X-ray scattering study of chicken erythrocyte chromatin.

The experimental evidence suggests that uncondensed "native" chromatin (i.e. chromatin with a full complement of histones) is best described by a helical structure with an extended pitch and that upon condensation the most significant structural modification is the reduction of this pitch.

We report here on the results of extensive model calculations on the chromatin superstructure. These calculations are applied to model the fully uncondensed "native" chicken erythrocyte chromatin superstructure and the most condensed state achieved just prior to precipitation.

The motivation behind this work was to provide a theoretical backing to the model derived in Perez-Grau et al. (1984) and in the accompanying paper by showing that the calculated solution scattering patterns display the features observed experimentally.

Solution scattering (Guinier and Fournet 1955) and helical diffraction theory (Klug et al. 1958) was used. We have approximated the structure by using spheres of appropriate diameters and densities. The solution scattering patterns were calculated using either Debye's formula or from the calculated helical diffraction patterns with the intensities averaged at equal values of the S-vectors, in other words obtaining the solution scattering patterns from the fibre diffraction diagrams by disorientation of the fibres over all directions in real space. We define the solution scattering vector S as $2\sin\Theta/\lambda$, where 2Θ is the scattering angle and λ the wavelength of the radiation used. To obtain the solution scattering patterns from the helical diffraction diagram one averages out the calculated intensities in the R, Z reciprocal cylindrical coordinates used in helical diffraction theory (see, for instance, Vainshtein, 1966 for detailed definitions) at equal values of S. The relationship between S and R, Z is simply: $S=\sqrt{R^2+Z^2}$. After averaging the intensities the resulting values were divided by $2\pi S$ to account for the dilution of intensities due to the disorientation. In the usual $I(S)*S$ versus S display for elongated particles in solution the inclusion of the $1/2\pi S$ correction factor is, of course, unnecessary. For a given structure both methods lead to identical results and it was only a matter of computational expediency which decided the approach we used at any one time.

2. The model for the nucleosome

In order to reproduce the features observed in the solution scattering patterns at resolutions greater than 10.0 nm it proved necessary to devise a reason-

* Present address: Instituto de Biologia de Barcelona, Juan de la Cierva, C. Jorge Girona Salgado s/n, Barcelona, Spain

ably realistic model for the nucleosome which at the same time was computationally tractable. We settled for a model consisting of 1.8 turns of a helical ring, made up with spheres of 2.25 nm diameter with a centre to centre distance of 1.7 nm. The helical diameter of the ring and its pitch are 8.5 and 3.4 nm respectively. The inner part of this ring is filled with 8 spheres of about 3.2 nm diameter evenly distributed within a cylinder of 5.7 nm height and 6.0 nm diameter. These dimensions for the spheres are small enough to avoid noticing significant effects due to their form factor within our range of measurements.

In order to simulate the excess electron density of nucleic acid over protein relative to water, the spheres in the helical ring were given a density 1.63 times larger than that of the spheres placed in the inner part, this factor was arrived at from the known electron density of water (0.33 e/A^3), the mean electron density of protein (ca. 0.44 e/A^3) and of DNA (ca. 0.51 e/A^3), defining the electron density of protein above water as unity, it follows that the density of nucleic acid is around 1.6 times higher. The factor was adjusted to give a calculated solution scattering pattern for the nucleosome which fitted well the measurements of Damaschun et al. (1980). This model, based on the known structure of the nucleosome core (Finch et al. 1981; Bentley et al. 1981; Richmond et al. 1984) yields a solution scattering pattern (not shown) in good agreement with the X-ray scattering (Damaschun et al. 1980) and neutron data (Hjelm et al. 1977; Richards et al. 1977) for mononucleosomes in solution to resolutions of around 4.0 nm.

Some of the features observed in the X-ray scattering patterns of mononucleosomes (Damaschun et al. 1980) are also observed in the solution scattering patterns of chromatin fibres (i.e. bands near 0.27 nm^{-1} and 0.36 nm^{-1}, shoulder at 0.15 nm^{-1} and prominent through near 0.22 nm^{-1}, Fig. 4c), and can be interpreted on the basis of these calculations as due to the maxima of the J_0 like Bessel function yielded by the transform of the DNA ring, but with their relative intensities modulated by the contribution of the inner protein component. In fact, the positions of these maxima closely follow the relationship $1/D * 1.22$, $1/D * 2.26$, $1/D * 3.23$ expected for such a function for $D = 8.35$ nm (i.e. 0.146 nm^{-1}, 0.27 nm^{-1} and 0.037 nm^{-1}, respectively). In line with previous work we consider that these bands in the scattering pattern of chromatin fibres as well as the trough at 0.22 nm^{-1} are mainly due to the nucleosome transform. The observation that the position and intensity of the trough are unaffected by the condensation process is a further indication in favour of this assignment.

The entrance and exit of the linker-DNA in the nucleosome were constrained so that it emerged on a straight path from the core DNA. As the linker-DNA describes 1.8 turns of a helical ring around the protein core (Bentley et al. 1981), it enters and emerges at points close to each other on its periphery and is allowed to extend by a length of ca. 22 nm (i.e. ca. 65 base pairs).

3. Modelling of uncondensed chicken erythrocyte chromatin in solution

The nucleosome equivalent sphere has a diameter of 10.4 nm (Hjelm et al. 1977; Richards et al. 1977; Damaschun et al. 1980); consequently, the maximum diameter for the equivalent solid cylinder of the "string of beads" model is 10.4 nm (i.e. with the nucleosomes packed on top of each other in a linear arrangement). Thus, the maximum value of the radius of gyration of the cross-section would be around 3.6 nm, which is compatible with the measurements on chromatin fibres extended by binding ethidium bromide but far smaller than the value for "native" uncondensed chromatin. These considerations provide a theoretical reason for dismissing the "string of beads" model as a possible structure for the uncondensed chromatin fibre in solution.

The presence of a prominent band at 0.05 nm^{-1} (Fig. 4c) indicates that significant contrast exists in the fibre, consequently even at low resolution the structure cannot be regarded as a solid cylinder and the radius of gyration of the cross-section cannot be directly related to the structure without resorting to modelling.

A helical structure is fully determined by a knowledge of the helical radius, the pitch, the number of subunits per turn, the orientation of the subunits relative to the helical axis and, of course, the structure of the subunit. However, at low resolution it is valid to approximate the subunit (i.e. the nucleosome) with the nucleosome equivalent sphere (i.e. a sphere with 10.4 nm diameter), which dispenses with the last two requirements and then build a model which is compatible with the observations.

The experimental observations show that the position of the maximum intensity and of the intensity onset of the 0.05 nm^{-1} band are subject to some variability. The position of the maximum ranged between 0.048 and 0.052 nm^{-1}, while its onset varied between 0.028 and 0.032 nm^{-1}. We believe that this variability simply illustrates the sensitivity of the structure to the preparative conditions. However, in the majority of the cases the onset and the top of the band appeared at 0.03 and 0.05 nm^{-1} respectively

and because of it, we use these values in the modelling that follows.

The shape of solution scattering bands can give a clue about their origin in the corresponding diffraction diagram. In the disoriented diffraction diagram a layer line with a meridional intensity will result in a step-like contribution in the $I(S) * S$ versus S plot of the solution scattering pattern, while an equatorial contribution will be characterized by a symmetric band. Between these two extremes there is a gradation in the steepness of the leading edge. In the case of a layer line with a near-meridional band, the Z-value of the layer line coincides with the S-value at the onset of the intensity step, rather than with its maximum. the S-value of the maximum gives a measure of the spacing between the electron density grooves in the fibre.

Using the criteria above one can conclude that the 0.05 nm^{-1} band might originate from a layer line with a near-meridional peak intensity and that its maximum is due to a persistent internucleosomal distance of around 20.0 nm. From the position of its onset one can estimate a helical pitch of the order of 33 nm.

It is straightforward to show that there is a relationship, involving the distance between successive subunits (d), the helical radius (r), the helix pitch (p) and the number of subunits per turn (N), given by

$$r^2 = \frac{d^2 - (p/N)^2}{2\left[1 - \cos\left(\frac{2\pi}{N}\right)\right]}.$$

A range of calculations in which d was varied around 20.0 nm were performed. An example of these calculations is shown in the right hand panel of Fig. 1, where the dependence of the helical radius as a function of the pitch for several values of N is shown. These results simply illustrate how in a helical structure, in which the constraint of a fixed distance between successive subunits has been imposed, there is a minimum pitch given by the constraining distance, in which case there is only one subunit per turn and the helical radius must be zero. This corresponds to the "string of beads" model. As one allows this structure to coil (i.e. one progressively increases the value of N) one can devise an infinite number of helical lattices. For low values of N (e.g. 1.25) one can have fairly large radii (notice that the curve crosses over those for larger values of N) and very low values of the pitch. Model calculations on this type of structure indicated that while it is possible to construct a model yielding the correct radius of gyration of the cross-section, it is not possible to make it yield a band at 0.05 nm^{-1}. For the model calculations to display a band in the neighbourhood of the correct position it proves necessary to invoke a helical pitch of ca. 33.0 nm (which in anycase is intuitively obvious from the considerations above). The problem then is to relate the helical radius to the radius of gyration of the cross-section, which will depend on the distribution of the mass along the fibre (i.e. N).

The left hand panel of Fig. 1 shows the relationship between the helical radius and the radius of gyration of the cross-section for models in which the

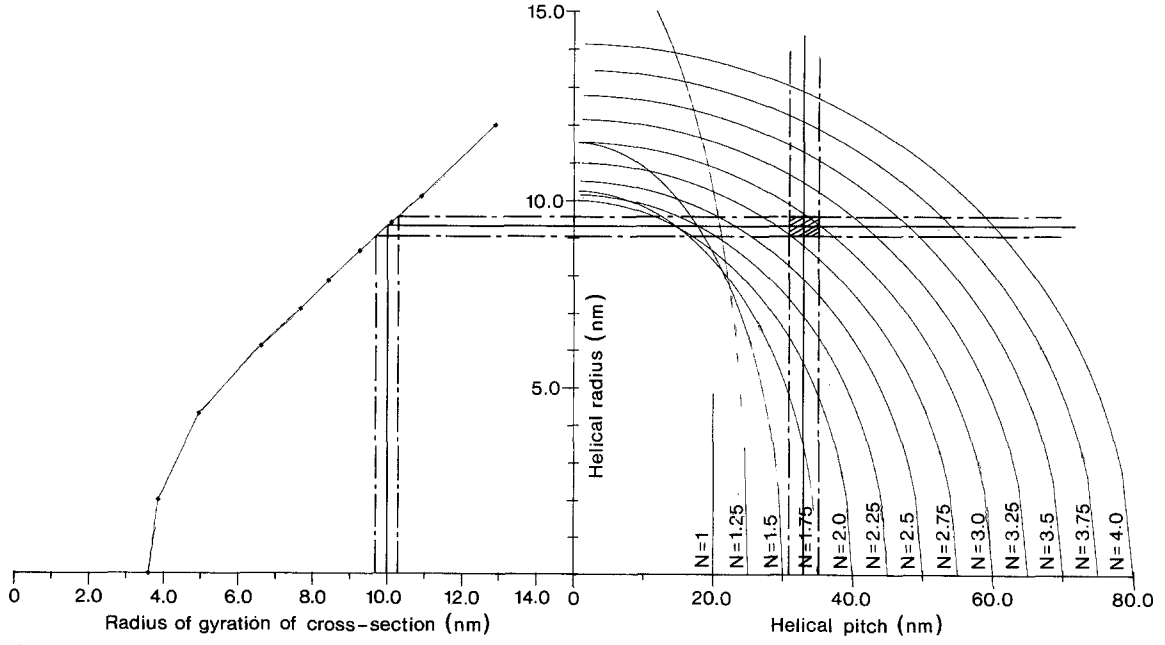

Fig. 1. Illustration of the approach used for the derivation of the most likely helical parameters describing the superstructure of uncondensed chicken erythrocyte chromatin fibres. (N changes from 1 to 4, in steps of 0.25)

pitch has been kept at 33.0 nm and N is progressively increased. The bands running across both panels correspond to the measured radius of gyration of the cross-section and the position of the onset of the rising edge of the 0.05 nm^{-1} band plus and minus their variability. The area of intersection defines the only possibilities compatible with the measurements. One converges to the most likely model for uncondensed chromatin as (on average) being a helical structure with a helical radius of ca. 9.3 nm, a pitch of ca. 33.0 nm and with ca. 2.9 nucleosomes per turn.

Figure 2a shows a model calculation of the corresponding solution scattering pattern. The pattern displays features that are in qualitative agreement with the observations, it has the correct radius of gyration of the cross-section, displays a minimum at 0.03 nm^{-1} and a broad asymmetric band with a maximum at 0.05 nm^{-1}. However, other less prominent bands appear superimposed on it. These bands are due to the contribution to the solution scattering pattern from subsequent layer lines. These bands were not detectable in the experimental results (Fig. 4c), this could be partly due to poor statistics but more likely to a certain variability in the structural parameters of the fibres in solution (i.e. diameter, pitch, number of subunits/turn). In other words, chromatin in solution should not be regarded as a rigid helical structure in the crystallographic sense. In fact the variability in the position of the maximum at about 0.05 nm^{-1} and of its onset is an indication of the structural lability.

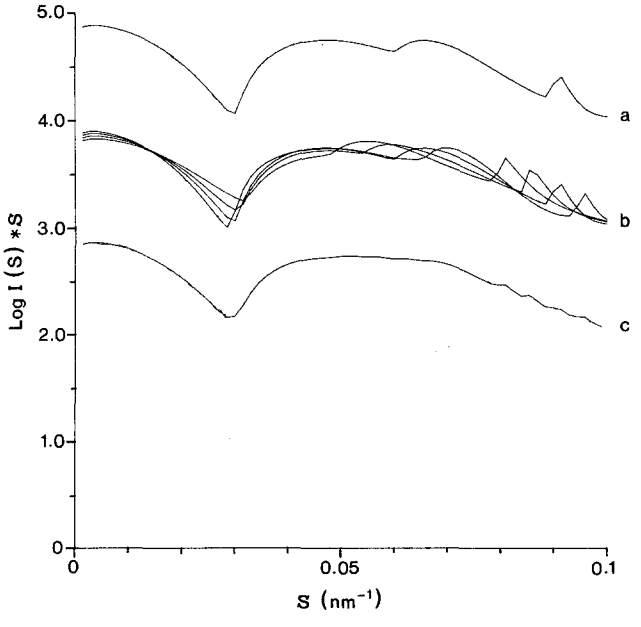

Fig. 2. **a** Calculated solution scattering pattern for a model of the uncondensed chromatin fibres consisting of a helix with 2.9 subunits per turn, a helical radius of 9.3 nm and a pitch of 33.0 nm. **b** Illustrates the effects due to slight variation in the helical parameters on the solution scattering patterns. **c** Shows the type of scattering pattern expected if the structures considered above coexisted in the solution

Figure 2b shows a series of calculated solution scattering patterns in which the pitch of the helix has been allowed to vary between 31.0 and 34.0 nm by varying N between 2.5 and 3.25 in steps of 0.25 and then using the corresponding helical radii in the calculations as derived above (i.e. 8.1, 8.8, 9.5 and 10.3 nm respectively). Notice that the weak bands come noticeable out of alignment, while the strong maximum remains, illustrating that only the diffraction maxima arising from the most prominent electron density grooves show up if a measure of disorder is included. Figure 2c corresponds to the average pattern, notice that while the trough at 0.03 nm^{-1} and the broad asymmetric band at 0.05 nm^{-1} persist, the weaker bands are eliminated. This illustrates one of the features of X-ray solution scattering, in the sense that it provides structural information about the average structure and consequently only those features that are common to every particle in the solution will show up in the X-ray scattering pattern.

The results shown in Fig. 2 also illustrate that variations in the values of the pitch of a few nm or changes in the number of subunits per turn of up to 20%–30% do not affect the shape of the scattering curves to the point that they would be incompatible with the experimental results.

To summarize, the calculations above provide support for a helix-like low resolution model of uncondensed chromatin, in which the number of subunits per turn is around 3, with a pitch of ca. 33 nm and a helical radius around 9.3 nm.

The question now is whether these helical parameters yield a calculated solution scattering pattern which at higher resolution is compatible with the observations. With the helical parameters derived above, the linker DNA must run almost straight along the inside of the helix from one nucleosome to the next.

We incorporated the nucleosome core model into this helical arrangement. As illustrated in Fig. 5a, we chose to place the path of the linker DNA so that it runs from the bottom of one nucleosome to the top of the next one along the helix. The DNA then winds 1.8 turns around the protein core and the next stretch of linker emerges at the bottom to join the top of the next nucleosome. Our data do not provide any evidence for this arrangement, but it reconsiles the need for continuity in the DNA with the distance between nucleosomes (i.e. the 0.05 nm^{-1} band) while retaining the overall helical symmetry and it fits with the geometry for the crystallographic model of the core DNA (Bentley et al. 1981).

Some calculated solution scattering patterns are shown in Fig. 4a. The linker DNA was kept at a length of 21.7 nm, with 2.75, 3.0 and 3.25 nucleosomes per turn which leads to radii of 8.8, 9.5, 10.5 and pitches of 32.3, 33.3 and 34.3 nm respectively. They correspond to helical lattices similar to those used in Fig. 2. The models reproduce the most prominent features observed throughout the range of measurements, i.e. maximum at 0.05 nm^{-1}, shoulder at ca. 0.15 nm^{-1}, trough at 0.22 nm^{-1} and bands at ca. 0.26 and 0.36 nm^{-1}. Other less prominent features are obtained. Their origin, as described above, is due to the contribution from higher order layer lines to the solution scattering patterns (a total of 170 layer lines were included in the calculations). As shown in Fig. 2b, small variations in the helical parameters are sufficient to suppress them. With the proviso that some form of disorder has to be considered the agreement between the model calculations shown in Fig. 4a, and the experimental results is good enough to give confidence in the proposed structure for uncondensed chromatin in solution.

Figure 4d provides a comparison with the data (Fig. 4c). A model consisting of a helical structure with a radius of 10.5 nm, a pitch of 34.3 nm and 3.25 subunits per turn was used in this calculation, the minima have been suppressed to a level comparable to the experimental observations by simply adding a monotonic $1/S^2$ function amounting to about 5% of the scattered intensity at the position of the 0.05 nm^{-1} maximum. This is intended to show that a monotonic background due to some disordered material is sufficient to eliminate the pronounced minima yielded by the model calculations. Notice that all the features observed experimentally are reproduced in the calculations, their relative intensities are in reasonable semi-quantitative agreement.

One immediate consequence of this model is that the position and intensity of the 0.05 nm^{-1} band should be strongly dependent on the length of the linker DNA. This raises the important issue that this model may only apply to certain types of chromatin. Preliminary X-ray scattering data for different chromatins appear to verify this point.

4. Modelling of condensed chicken erythrocyte chromatin in solution

At low resolution, the condensed chromatin fibre can be regarded as a cylinder in which the nucleosomes form its wall and its inside is filled with the linker DNA and the fifth histones.

In such a structure, the very low angle region of the solution scattering pattern is directly related to the equatorial intensity in the corresponding fibre diffraction pattern by:

$$I(S) * S = 2\pi \left[(\varrho_i - \varrho_0)\, r_i^2 \frac{J_1(u_i)}{u_i} + \varrho_0 r_0^2 \frac{J_1(u_0)}{u_0} \right]^2$$

where:

$u_i = 2\pi r_i R$ and $u_0 = 2\pi r_0 R$,

where r_0 and r_i are the outer and inner radius respectively and ϱ_0 and ϱ_i the corresponding electron densities. J_1 is a first order Bessel function and R is the abscissa in the $R-Z$ fibre diffraction diagram. Independently of whether the inner and outer electron density differ or not this formula predicts a subsidiary maximum at low angles which is directly related to the diameter of the particle. However, the expected prominence of this maxima depends on the differences of density, the higher the difference the more prominent the maximum.

The measured 13.5 nm radius of gyration of the cross-section for condensed chromatin implies that the corresponding equivalent solid cylinder would have a diameter of ca. 38.0 nm (Kratky and Porod 1953) while the equivalent hollow cylinder would have a mean diameter of ca. 27.0 nm. In either case one should obtain a subsidiary maximum at around 0.045 nm^{-1}. The patterns display such maximum. Because of its weakness it should be taken as an indication that one can regard condensed chromatin as a near solid cylinder.

Whatever the case, one can derive a value of the helical radius from the position of this band. Model calculations using the formula above indicate a helical radius of ca. 13.5 nm, which coincides with the value for the radius of gyration of the cross-section (see accompanying paper). This is not surprising because if one regards the fibre as hollow then the radius of gyration of the cross-section coincides with the helical radius and if it is considered to be a solid cylinder, the helical radius would be given by the difference between the outer radius (i.e. 19.0 nm) and half a nucleosome length, which leads also to 13.5 nm.

Whether one uses a solid cylinder or a hollow one, the formula predicts a maximum at ca. 0.045 nm^{-1}. However, the minima yielded by the formula are true zeroes and should show up prominently in the measurements if the structure was rigidly determined. Suppression of minima (i.e. zeroes in the transform of the structure) is common in solution scattering. One can suggest several effects that might contribute to their suppression, for instance: as there is a distribution of lengths in the fibres one expects a coherent length effect from the the shorter ones, this phenomenon will be more

noticeable for condensed than for uncondensed chromatin because of the reduced fibre length. Another contributory factor is polydispersivity in the fibres as some of them are likely to be more condensed than others (i.e. a variability in diameter). Dynamic fluctuations or bending of the fibres will also tend to suppress the zeroes. We cannot ascertain from the data which effect might be mainly responsible for the suppression of the scattering zeroes as they are all likely to contribute.

Consequently, on the basis that it yields the correct radius of gyration and a band at 0.045 nm^{-1}, one can describe the low resolution structure of condensed chromatin as a solid cylinder with an outer diameter of ca. 38.0 nm. However one has to invoke a departure from a rigidly defined structure in order to explain the absence of well defined minima in the scattering patterns.

The observations (Fig. 4 e) show that there are only two prominent bands associated with the packing of the nucleosomes appearing during condensation, namely, the 0.09 and the 0.16–0.17 nm^{-1}. The bands correspond to spacings of of ca. 11.0 and 6.0 nm which closely match the known dimensions of the nucleosomes. As no other bands are observed to develop, this suggests that the nucleosomes pack in the condensed fibre leaving no prominent electron density grooves other than those due to the nucleosomes coming into contact with each other. We show below that a reduction of a helical pitch of the uncondensed fibres by a factor of eight or more reconciles the need for close packing with the appearance of bands only in the observed positions.

The suggested structure for the uncondensed fibre cannot achieve the observed increase of mass per unit length by a simple reduction of its pitch without the nucleosomes unreasonably penetrating each other. However, a slight helical overwinding is sufficient for the cores to become aligned so that, upon reduction of the pitch, they fit next to each other along the periphery of the fibre with the required degree of compaction.

Overwinding the nucleosomes around the fibre axis is equivalent to a reduction of the number of subunits per turn (N). If one assumes that the length of the linker DNA remains constant and that, initially at least, the pitch of the helix does not decrease significantly then it unavoidably follows that the helical radius must decrease (Fig. 1). The drop in the radii of gyration of the cross-section detected at low to intermediate ionic strengths may be due to this effect (see accompanying paper).

Such a structural change can lead to an infinite number of helical lattices for the condensed chromatin fibre. There are, however, some independent constraints that can be applied in its modelling which help to converge towards a most likely helical lattice, namely:

(*a*) Electric field dichroism measurements indicate that the nucleosomes have to be inclined about 30° relative to the fibre axis (Mitra et al. 1984).
(*b*) The linker DNA has to be inclined at about 45° relative to the fibre axis (Mitra et al. 1984).
(*c*) The length of linker DNA must not exceed the equivalent of ca. 64 base pairs.
(*d*) Upon reduction of the helical pitch an increase of mass per unit length greater than 8 times relative to the uncondensed chromatin model must be obtained.
(*e*) The value of the radius of gyration of the cross-section of the resulting model must be 13.5 nm.
(*f*) Upon reduction of the helical pitch, the calculated solution scattering pattern must display a series of bands near 0.045, 0.08–0.09, 0.16–0.17, 0.27 and 0.37 nm^{-1}, a trough at 0.22 nm^{-1} and an overall background increase centered at around 0.35 nm^{-1}.
(*g*) The relative intensities of these bands must be at least in semi-quantitative agreement with the experimental observations.
(*h*) Folding should be achieved without interpenetration of the nucleosomes and/or of the linker DNA.
(*i*) The structure should explain why a chromatin fragment containing 6 nucleosomes should have a significantly higher sedimentation rate than chromatin fragments containing 5 or less nucleosomes (Butler and Thomas 1980; Thomas and Butler 1980).

We considered the surface lattices obtained by overwinding the uncondensed fibre and then reducing the pitch until an eightfold increase in mass per unit length is achieved.

Figure 3 illustrates the procedure. The helical radius is fixed at 13.5 nm and the nucleosomes (represented by rectangles with dimensions of $11 \times 5.7\ nm^2$) are placed with their long axis inclined by 30° relative to the fibre axis to account for the electric field dichroism measurements. Many of the lattices can be dismissed because in order to achieve the desired degree of compaction the nucleosomes have to interpenetrate each other (depicted in Fig. 3 by the shaded areas). Using this topological criterion the following ranges of allowed values for the number of subunits per turn (N) were defined: $2.74 > N > 2.54$, $2.36 > N > 2.34$, $2.27 > N > 2,16$, $1.83 > N > 1.67$ and $1.29 > N > 1.07$. Notice that these lattices include many of those suggested in the literature (see for instance: Staynov 1983 and references therein).

Since the structure also has to be compatible with the results of Butler and Thomas (1980) and

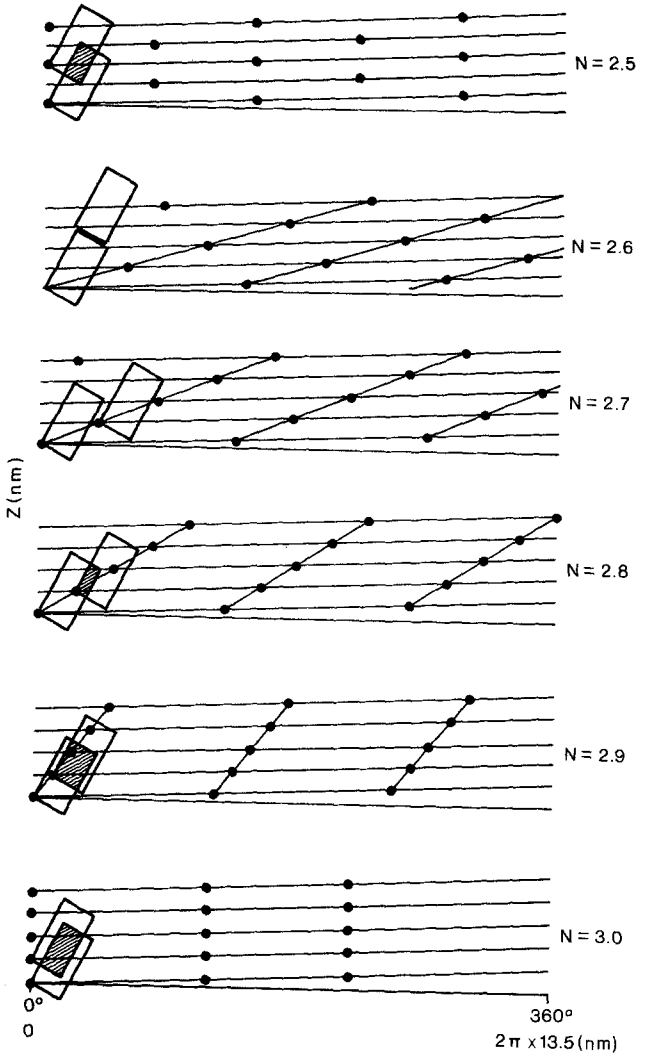

Fig. 3. Illustrates the procedure for the deduction of an approximate helical lattice for condensed chromatin

Thomas and Butler (1980) one must converge towards a model in which the sixth nucleosome somehow stabilizes the structure leading to a choice of N in the range of 2.55–2.57 nucleosomes per turn. Notice that in this case the sixth nucleosome would make a side to side contact with the first, however with a fragment of five nucleosomes there is no connection and the structure would sediment more slowly.

We calculated the solution scattering patterns for a very large number of the surface lattices conceivable on the basis of the topological criterion. The best model corresponded to a helical structure of 13.5 nm helical radius, with pitches between 2.8 and 3.4 nm and with N at around 2.56 nucleosomes per turn.

Some calculated solution scattering patterns with helical parameters in this region are shown in Fig. 4b. The traces were obtained by fixing N at 2.56 and d at 21.7 nm and allowing p to vary from 2.8 to 3.4 nm in steps of 0.1 nm. In this situation the values of r remain very close to 13.5 nm.

Notice the presence of bands at around 0.045, 0.08 and 0.15–0.17 nm^{-1}, as well as a trough at about 0.22 nm^{-1}. There are also many other weak bands, particularly beyond 0.2 nm^{-1}. The absence of these bands in the experimental results can be accounted by relaxing the assumption that one is dealing with well defined rigid structures with an infinite coherent length. The model calculations show that the positions of these bands change for

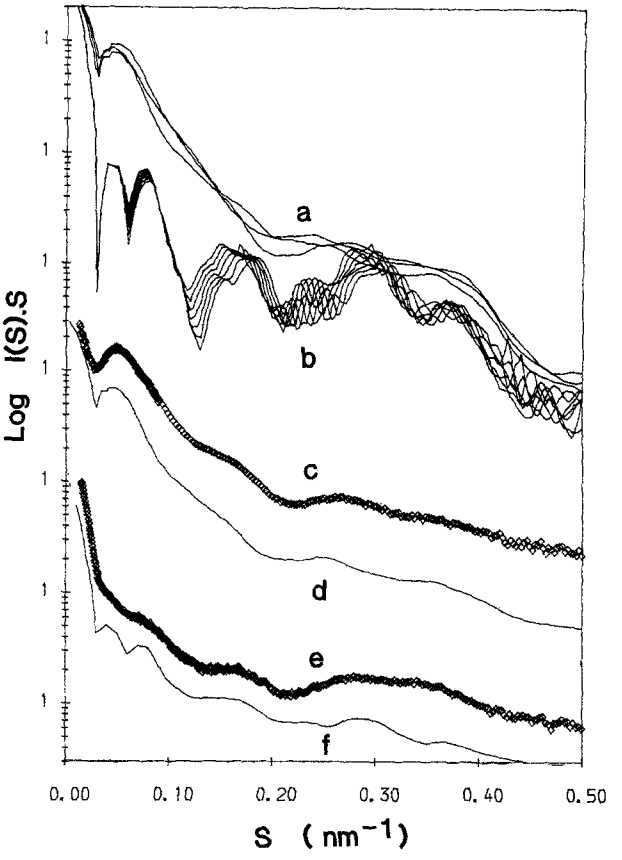

Fig. 4. **a** Calculated solution scattering patterns for models of uncondensed chromatin with the general characteristics of the structure illustrated in Fig. 5a. **b** Calculated solution scattering patterns for models with the general characteristics of that shown in Fig. 5d. **c** Experimentally recorded X-ray scattering pattern for uncondensed chicken erythrocyte chromatin. **d** Calculated solution scattering pattern for a helical model with a radius of 10.5 nm, a pitch of 34 nm and 3.25 nucleosomes per turn. A $1/S^2$ function has been added as a background in order to suppress the minima. **e** Experimentally recorded X-ray solution scattering pattern for condensed chicken erythrocyte chromatin. This pattern yielded a radius of gyration of 13.5 nm and an increase of mass per unit length of ca. 8 times relative to that shown in **c**. **f** Calculated solution scattering pattern for a helical model with a radius of 13.5 nm, pitch of 3.2 nm and 2.56 nucleosomes per turn. A $1/S^2$ function has been added to suppress the minima

slightly different helical symmetries. One can visualize the pattern resulting from a less ordered structure by simply considering the envelope of those shown. The envelope shows that only the bands at 0.045, 0.08–0.09, 0.15–0.017, 0.27, 0.37 nm^{-1} would persist, i.e. where observed experimentally (Fig. 4e for comparison), also, if disorder was included, then the average structure would yield an overall increase in the background, broadly centered at 0.35 nm^{-1}, which is a feature also observed experimentally.

The low angle bands in the calculations display minima which are more prominent than those observed. A reduction of the coherence length of the model or the inclusion of some disordered material contributing to a monotonic background would reduce the prominence of the minima.

Figure 4f provides an illustration of how by addition of a $1/S^2$ function, to represent the presence of disordered material, one can suppress the minima and yield bands at the observed positions with relative intensities in semi-quantitative agreement with the observations.

The fifth histone was not included in any of the model calculations. As it is complexed with the linker, it would be placed in the inside of the structure and reduce the prominence of some of the bands, particularly the 0.045 nm^{-1} band arising from the difference between the electron densities in the interior and the periphery of the structure.

The comparison between the model calculations and the experimental results show that whatever lattice the condensed fibre has adopted, there is no evidence for a rigidly determined structure of chromatin. Rather to the contrary, the data suggests a structure with a fairly high degree of disorder or the coexistence of closely related, but nevertheless different structural states in which the main topological relationships are conserved.

Notice also that the model calculations show that as the pitch is decreased from 3.4 to 2.8 nm, the bands at 0.08–0.09 and 0.16–0.17 nm tend to shift to higher angles. This mimics the experimental observations and, because when precipitation took place these bands were best defined and at the highest values of S, we take it as supportive evidence that maximal condensation coincides with precipitation.

Summary and conclusions

The model calculations above predict prominent diffraction bands where observed experimentally and by invoking a realistic measure of disorder in the helical parameters or the coexistence of a continuum of closely related helical lattices one can explain why the weak bands are not observed. They provide support for a model of the structure with the general characteristics described in Perez-Grau et al. (1984) and in the preceeding paper. According to the model we propose, whether condensed or uncondensed, chromatin in solution cannot be strictly regarded as helical but rather as helix-like and capable of adopting a continuum of closely related but nevertheless different configurations. This ability to accomodate a sufficiently wide variety of similar structures might be crucial to its function in as much as the latter requires folding and unfolding over regions of variable sizes.

It is hard to imagine that large rotations of the entire fibre can take place within the cell nucleus. If these are excluded, local unfolding of the chromatin has to be accompanied by the lengthening of the linker DNA and/or a rotation of the nucleosome cores. Conversely, local condensation must entail shortening of the linker DNA. These topological properties provide a wide range of possibilities for controlling the local structure of chromatin. In this respect it is perhaps significant that while ethidium bromide further uncondenses the chromatin-EDTA fibre by unwinding, thus lengthening, the DNA, its overwinding might achieve condensation.

These observations also provide possible hints about the action of site specific topoisomerases which by changing the DNA linking number, and consequently its length, might induce local unfolding and hence accessibility of the DNA for transcription.

At very high Mg^{++} concentrations the band at 0.045 nm^{-1} disappears. This band should be much reduced if the inner and outer electron density are equal. From the known molecular weights of the histones and of DNA and the values of the radii of gyration, one expects the outer density of partially condensed chromatin to be initially smaller, but to become equal to or bigger than the inner density as the fibre diameter increases. This may be an explanation for the observed disappearance of this band at high ionic strength.

From the fibre diffraction diagrams of the models one can establish that the solution scattering band near 0.08–0.09 nm^{-1} has a near-meridional as well as a near-equatorial contribution. In fact, equatorial and near meridional bands have been observed on partially ordered calf thymus chromatin containing the five histones (Baldwin et al. 1978). The off-meridional band was interpreted as arising from the pitch of the helical arrangement whereas the equatorial one, clearly visible in the data, was not interpreted. Our model calculations suggest that a similar pattern would be obtained from partially oriented chicken erythrocyte chromatin.

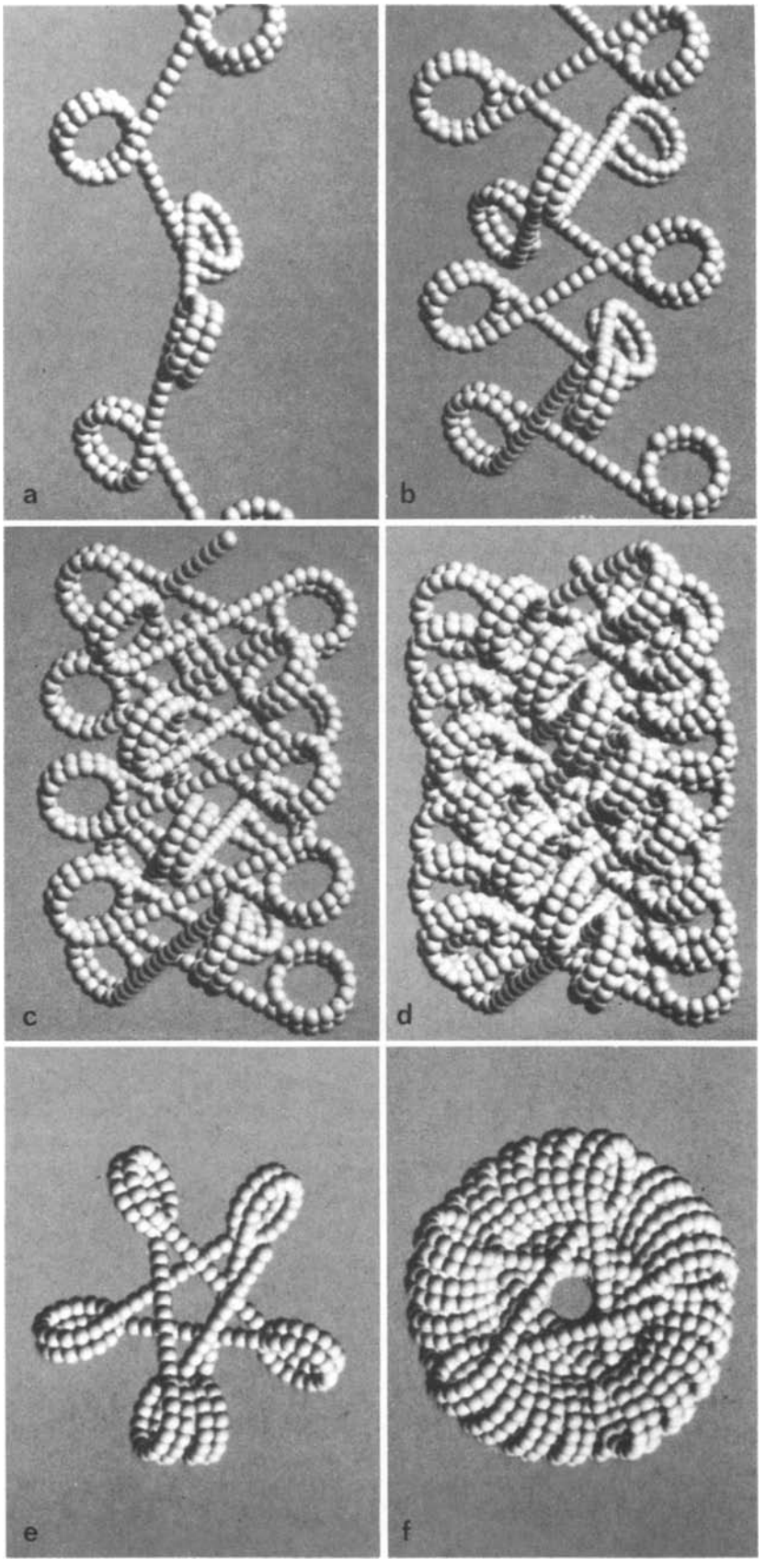

Fig. 5a–f. Summary of the main conclusions. Structures with the general characteristics of the ones displayed here yielded calculated solution scattering patterns compatible with the experimental observations. **a** Suggested structure of uncondensed chromatin. **b** and **c** Partially condensed chromatin derived by reduction of the helical pitch of the structure shown in **a**. **d** Suggested structure of condensed chromatin. **e** Illustration of the structural basis of the jump in the sedimentation properties for lengths greater than 6 nucleosomes. Notice how after 2 turns the sixth nucleosome makes contact with the first. **f** A view down the fibre axis of the condensed chromatin model

The solution scattering band near $0.16-0.17\,nm^{-1}$ also contains a mixture of layer lines and near equatorial contributions, arising from the side to side packing of the nucleosomes. In fact, the almost 2 : 1 ratio in the maximal outer dimensions of the nucleosomes will unavoidably lead to the appearance of overlapping bands in the solution scattering pattern.

The computer generated models shown in Fig. 5 are intended to provide a summary of the main structural conclusions of this work. They illustrate what we believe are the more salient features of the superstructure of chromatin.

Only the DNA chain is displayed in the graphics. Each nucleosome is represented by a string of spheres which loop around 1.75 turns of a helical ring with the dimensions given in Sect. 6. The centre to centre distance between successive spheres is equivalent to 1.7 nm and a total of 42 spheres were used to construct the nucleosome core and its associated linker. Given these dimensions one sphere can be regarded as roughly corresponding to half a pitch of the DNA double helix. In this representation the 42 spheres correspond to ca. 210 base pairs of DNA, 64 of which make the linker chain.

The linker DNA is represented as a straight rod, although there is, of course, no definite proof for it, except perhaps in the case of uncondensed chromatin where it would be difficult to explain the presence of the $0.05\,nm^{-1}$ band if this was not the case. In the model the linker is made to run from the bottom of one nucleosome to the top of the next one. This arrangement was necessary not only to satisfy the topological constraints, but also because of the requirement that the linker should present an angle of ca. 45° relative to the fibre axis (Mitra et al. 1984).

Figure 5a shows the model for uncondensed chromatin. Some features are worth mentioning: when viewed on a sideways projection as displayed, there are stretches with the appearance of the "zig-zag" structure often reported in electron microscopy studies. The model tends to show a sequence of two nucleosomes close to each other with more distal neighbours on either side and may give the impression that in some cases the linker enters and emerges at the same point in the nucleosome while in other cases it does so on opposite sites. These features are displayed in electron micrographs from spread chromatin (see for instance Moyne et al. 1981) and we believe that this is simply a consequence of how the structure is viewed, which in the case of electron microscopy will depend entirely on how the fibre has settled on the grid. The proposed model is thus entirely compatible with the electron microscopy results.

Notice that if this structure undergoes a reduction of its helical pitch while the linker DNA remains more or less straight its diameter will increase.

Figures 5b and c illustrate partial states of condensation which according to our results would approach the situation at physiological salt conditions.

Finally, Fig. 5d is the model closely representing what we believe is the almost completely condensed chromatin. The model shown in the figure can still be made to condense further but in order to do so the linker-DNA has to bend, also the cores may have to change the angle they present to the fibre axis. There is sufficient room to accomodate the fifth histone inside this structure.

Figure 5e shows a view down the fibre axis and illustrates how after the first two turns the sixth nucleosome makes contact with the first one, thus stabilizing the fibre. Notice that it is conceivable that under certain conditions this stable unit may remain in stretches of the fibre, while in other regions the fibre may be partially or totally uncondensed. If this situation took place, then this structure provides the means to reconcile the "superbeads" model (Renz et al. 1977; Hozier et al. 1977) with the "solenoid" model (Finch and Klug 1976).

Figure 5f provides a view down the fibre axis after many turns. Although the interior is fairly full, there is a small hole left in the centre. However, in order to explain the weakness of the 0.045 nm band, it is necessary to assume that the interior is probably totally occupied by the linker DNA and the fifth histones.

In the absence of well oriented chromatin fibres, which we are presently trying to obtain, it is, of course, impossible to guarantee the uniqueness of the model. However, given the experimental observations and the fact that these model calculations provide a reasonable agreement with the patterns, we believe the evidence in its favour is sufficiently strong to suggest that it represents many of the features of the structure of chromatin in solution. Thus, although one should not consider the model as uniquely established we hope that it can provide a useful framework for the description of the superstructure of chromatin.

Acknowledgements. We would like to thank the staff at the European Molecular Biology Laboratory Outstation of Hamburg and at Daresbury Laboratory for their support during the course of this work. Particularly, we thank G. R. Mant, S. Zurek and E. Pantos for making available their computer graphics package (to be published) which proved invaluable in the visualization of the fulfillment of the topological constraints in the model structures.

This work was supported by a grant from the Deutscher Akademischer Austauschdienst (DAAD) to M.C. Vega.

L. Perez-Grau was the recipient of an EMBL postdoctoral fellowship.

References

Baldwin JP, Carpenter BG, Crespi H, Hancock R, Stephens RM, Simpson JK, Bradbury EM (1978) Neutron scattering of chromatin in relation of higher-order structure. J Appl Crystallogr 11:484–486

Bentley GA, Finch JT, Lewit-Bentley A (1981) Neutron diffraction studies on crystals of nucleosome cores using contrast variation. J Mol Biol 145:771–784

Butler PJG, Thomas JO (1980) Changes in chromatin folding in solution. J Mol Biol 140:505–529

Damaschun H, Damaschun G, Pospelov VA, Vorob'ev VI (1980) X-ray small angle scattering study of mononucleosomes and the close packing of nucleosomes in polynucleosomes. Mol Biol Rep 6:185–191

Finch JT, Klug A (1976) Solenoidal model for superstructure in chromatin. Proc Natl Acad Sci USA 73:1879–1901

Finch JT, Brown RS, Rhodes D, Richmond T, Rushton B, Lutter LC, Klug A (1981) X-ray diffraction study of a new crystal form of the nucleosome core showing higher resolution. J Mol Biol 145:771–784

Guinier A, Fournet G (1955) Small angle scattering of X-rays. John Wiley, New York

Hjelm RP, Kneale GG, Suau P, Baldwin JP, Bradbury EM, Ibel K (1977) Small angle neutron scattering studies of chromatin subunits in solution. Cell 10:139–151

Hozier R, Renz M, Nehls P (1977) The chromosome fibre: Evidence for all ordered superstructure of nucleosomes. Chromosoma 62:301–317

Klug A, Crick FHC, Wyckoff HW (1958) Diffraction by helical structures. Acta Crystallogr 11:199–213

Kratky O, Porod G (1953) Die Physik der Hochpolymere, vol 2. Springer, Berlin Heidelberg Göttingen

Mitra S, Sen D, Crothers DM (1984) Orientation of nucleosomes and linker DNA in calf thymus chromatin determined by photochemical dichroism. Nature 308:247–250

Moyne G, Freeman R, Saragosti S, Yaniv M (1981) A high resolution electron microscopy study of nucleosomes from simian virus 40 chromatin. J Mol Biol 149:735–744

Perez-Grau L, Bordas J, Koch MHJ (1984) Chromatin superstructure: Synchrotron Radiation X-ray scattering study on solutions and gels. Nucleic Acid Res 6:2987–2995

Renz M, Nehls P, Hozier J (1977) Involvement of histone H1 in the organization of the chromosome fiber. Proc Natl Acad Sci USA 74:1897–1883

Richards B, Pardon J, Lilley D, Cotter R, Wooley J, Worcester DL (1977) The sub-structure of nucleosomes. Cell Biol Int Rep 1:107–116

Richmond TJ, Finch JT, Rushton B, Rhodes D, Klug A (1984) Structure of the nucleosome core particle at 7 A resolution. Nature 311:532–537

Staynov DZ (1983) Possible nucleosome arrangements in the higher order structure of chromatin. Int J Biol Macromol 5:3–9

Thomas JO, Butler PJG (1980) Size-dependence of a stable higher order structure of chromatin. J Mol Biol 144:89–93

Vainsthein BK (1966) In: Diffraction of X-rays by chain molecules. Elsevier, Amsterdam